Thermal Study of Induction Motors by Phantom Loading Using Multi-slice Time Stepping Finite Element Modeling

S. L. Ho W. N. Fu *H. C. Wong
Department of Electrical Engineering *Industrial Centre
The Hong Kong Polytechnic University, Kowloon, Hong Kong

Abstract — **It is difficult to test large induction motors without expensive facilities or suitable loading. This paper reports the findings in an attempt to assess the thermal properties of commercial induction motors by injecting phantom load currents into the windings. A multi-slice 2-D time stepping finite element model is used to analyze the loss distributions in the machine with phantom loading and with normal direct loading. It can be shown that the high-order harmonic losses in the motor can be precisely estimated with the proposed method. Both experimental and simulation results confirm that phantom loading can be used as substitutes of direct full-load temperature-rise test of induction motors.**

Index terms – **Induction machines, testing, losses, finite element methods.**

I. Introduction

Many large induction motors cannot be tested or loaded fully even after commissioning due to the absence of a suitable load, since it is common for the users to order over-sized motors to cater for future expansion. In many cases the motor cannot readily be coupled mechanically with the load *in situ*, especially when the motor is installed vertically. Even if the load is available, it might also be too late to reject a fully commissioned motor if it runs too hot on full load. Full-load temperature-rise test results will also be useful for the engineers to plan their servicing schedule. Hence it will be interesting to find some indirect means to study the temperature-rise of induction motors when the actual load is not available or when the motor cannot be loaded readily.

Some researchers have proposed to use special phantom load tests to produce the rated losses in the machines without a real load on the motor shaft [1-2]. In those methods some special connections are required and d.c. current is injected into the windings in order to produce the rated losses in the motors. Note however that even if the total losses at rated conditions can be injected into the machine in an indirect load test, the distribution of the losses in the various locations could be different. The hot spots under phantom loading condition and under normal loading condition could then differ. Moreover, because of the presence of d.c. current in the stator windings under phantom loading, the magnetic fields in the air-gap will include two parts, one rotating at synchronous speed and one being stationary. Hence the distribution of losses in the motor could not be estimated precisely with traditional methods.

In this paper a comprehensive study using finite element method (FEM) is proposed and reported. In order to consider the skewed rotor bars as well, a multi-slice model is used. Time stepping method is used to solve the FEM equations, which are time dependent. Both the a.c. and d.c. fields are to be considered simultaneously. The computed losses will include the high-order harmonic losses because the time stepping method will consider the non-sinusoidal changes of currents and magnetic fields. The copper losses and the iron losses are also evaluated directly according to the results of the time stepping model. The computed results show that the loss distributions of phantom loading operations are very close to that of the actual full-load operating condition. The authors are glad to report that the thermal test results of an 11 kW skewed rotor induction motor under both phantom loading operation and full-load operation are very close to each other.

Manuscript received June 1, 1998.

S. L. Ho, (852) 27666170, fax 23301544, eeslho@inet.polyu.edu.hk, http://158.132.71.85/ W. N. Fu, (852) 2766 6135, eewnfu@polyu.edu.hk, http: //158.132.71.85.

The authors are grateful for the funding from the Hong Kong Polytechnic University to support this research project.

II. Phantom Loading Methods

Two identical motors are required for phantom load testing. Mechanical coupling between them is not necessary. The motors are only coupled to each other electrically. There is also no mechanical output from either motor.

Phantom loading with d.c. current flowing in the ratio of 1:1:1

One possible phantom loading connection [1] requires the motors to be re-connected essentially in star as shown in Fig. 1, even though most industrial-sized induction motors are connected in delta. Balanced 3-phase voltages are applied and the motor runs on no-load. The current directions of the d.c. being injected into the windings are shown in Fig. 1.

The beauty of this star-connection is its symmetry in both a.c. and d.c. circuits. The star points of the stator windings are at the same a.c. potential. The a.c. supply terminals are also at the same d.c. potential. The a.c. and d.c. sources can thus feed the two star-connected circuits at the same time independently. The phantom currents in all the three phases are identical. The disadvantage is that a voltage supply having $\sqrt{3}$ times the normal supply is required if the motors are normally connected in delta. Because of the requirement for an abnormally high voltage, it is sometimes difficult to find a suitable power supply, especially for large motors, to carry out the test.

Phantom loading with d.c. current flowing in the ratio of 1:1:0

The authors have however reported that there is another possible connection [2] to inject the phantom loading current

into the windings of a delta connected motor (Fig. 2). The current directions of the d.c. injected into the windings are shown in Fig. 2. It is necessary to insert three resisters R into the supply source to prevent the d.c. current from straying into the supply sources. The capacitor C is connected in parallel with the d.c. source to provide a path for the a.c. to feed into the auxiliary motor. Switch S_1 should be closed during the starting process although it should be open before any d.c. current is injected into the windings. The main motor will normally rotate at its no-load speed. The phantom d.c. currents flowing in the windings would then be in the ratio of 1:1:0 rather than 1:1:1.

Differences between phantom and direct loading

The air-gap m.m.f.'s under phantom loading (Fig. 3 (a) and (b)) are slightly different from that under normal operation (Fig. 3 (c)). However, with normal loading, the stator currents are at mains frequency and the rotor currents are at slip frequency. With phantom loading most of the stator current is d.c. although the rotor currents are around mains frequency. For a successful simulation it is necessary to show that the total motor losses under phantom loading are essentially the same as its rated losses. Although Fong [1] and Ho [2-3] did try to explain the basic principles of phantom loading using traditional methods, they could not precisely estimate the actual stray losses under phantom loading and under direct loading conditions. Developments in time stepping FEM of induction motors have however provided a possibility to analyze such complicated operations accurately [4].

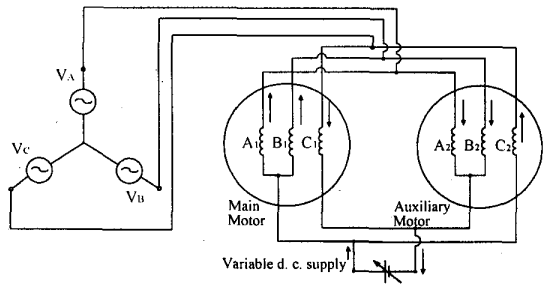

Fig. 1 Phantom loading connection for star-connected windings (1:1:1 method)

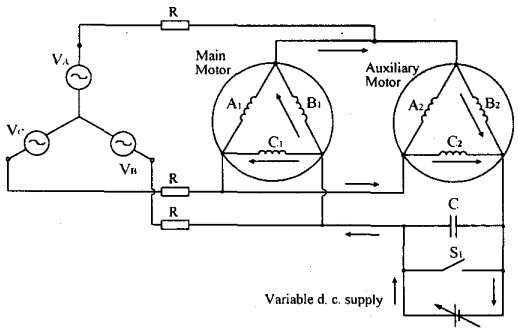

Fig. 2 Phantom loading connection for delta-connected windings (1:1:0 method)

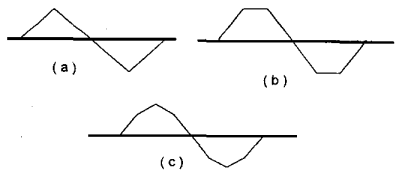

Fig. 3 (a) M.M.F. with phantom current identical in all three phases
(b) M.M.F. with phantom current in the three phases in the ratio of 1:1:0
(c) M.M.F. with normal balanced currents in the three phases

III. Modelling of Motor Operations

Both a.c. and d.c. are present and the two motors are coupled electrically together during the phantom load test. The FEM equations of the two motors are coupled together from the system's point of view. However, because the aim of the modeling is to compare the loss distributions between normal direct loading and phantom loading, the measured phase voltage waveforms can be used as the input data. Only the FEM equations of the main motor would need to be solved and the analysis is simplified as a voltage driven problem. The computation time can thus be shortened considerably.

Most commercial induction motors have skewed rotors and hence the modeling of such motors should therefore be three-dimensional (3-D). 3-D modeling is however well known for being computationally inefficient and hence the authors are proposing to use a 2-D multi-slice approach to model an induction motor under both normal operation and phantom loading. With such method the rotor is divided into M slices, with the bars in each slice offset from each other by $(1/M)^{\text{th}}$ of its total skewing angle. In each slice the magnetic vector potential has an axial component only. The current flowing in the rotor bars of each slice is forced to be the same as that flowing in the same bar of every other slice. The circuits of rotor end rings are also coupled into the FEM equations in such 2-D multi-slice models.

A stator circuit of one phase is shown in Fig. 4. The stator circuit equation of one phase is:

$$e + R_1 i + L_\sigma \frac{\mathrm{d}i}{\mathrm{d}t} = v_s \tag{1}$$

where R_1 is the total stator resistance of one phase winding; L_σ is the inductance of the end windings and the induced electromotive force is [5],

$$e = -\frac{l}{SM}\sum_{m=1}^{M}\left(\iint_{\Omega_+^{(m)}}\frac{\partial A}{\partial t}d\Omega - \iint_{\Omega_-^{(m)}}\frac{\partial A}{\partial t}d\Omega\right) \tag{2}$$

where the rotor is divided axially into M slices of equal length; m stands for the m^{th} slice; A is the axial component of the magnetic vector potential; l is the axial length of the stator iron core; S is the total cross-sectional area of one turn at one side; Ω_+ and Ω_- are, respectively, the cross-sectional areas of the 'go' and 'return' side of the phase conductors of the coils.

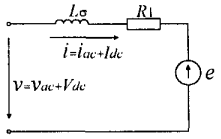

Fig.4 A stator circuit of one phase

The stator phase voltage v_s and the stator current i can be separated into their respective a.c. and d.c. components. Therefore, equation (1) becomes:

$$e + R_1(i_{ac} + I_{dc}) + L_\sigma \frac{\mathrm{d}(i_{ac} + I_{dc})}{\mathrm{d}t} = v_{ac} + V_{dc} \tag{3}$$

where i_{ac} and I_{dc} are the a.c. and d.c. components of i respectively; v_{ac} and V_{dc} are the a.c. and d.c. components of v_s, respectively.

Because the induced electromotive force e has no d.c. component, the d.c. current can be directly obtained from:

$$I_{dc} = (V_{ac} / R_1) \tag{4}$$

Substituting (2) and (4) into (3), the stator circuit equation is:

$$-\frac{l}{SM}\sum_{m=1}^{M}\left(\iint_{\Omega_+^{(m)}}\frac{\partial A}{\partial t}d\Omega - \iint_{\Omega_-^{(m)}}\frac{\partial A}{\partial t}d\Omega\right) + R_1 i_{ac} + L_\sigma \frac{di_{ac}}{dt} = v_{ac} \tag{5}$$

In the stator conductor domain, the field equation is:

$$\nabla \times (\nu \nabla \times A) - (i_{ac} / S) = (I_{dc} / S) \tag{6}$$

where ν is the reluctivity of the material.

Equations (5) and (6) give rise to the basic formulas in the stator conductor domain. Here v_{ac} and I_{dc} are the exciting sources, i_{ac} and A are the unknowns. Although in the stator circuit only the a.c. current is included, the magnetic field is excited by both a.c. and d.c. and hence the physical principles governing the motor operation will remain unchanged.

In the rotor conductor domain, the governing equations are the same as that for a normal motor [5],

$$\nabla\times(\nu\nabla\times A)+\sigma\frac{\partial A}{\partial t}+\frac{\sigma}{MS}\sum_{m=1}^{M}\iint_{\Omega^{(m)}}\frac{\partial A^{(m)}}{\partial t}d\Omega-\frac{\sigma}{S}\iint_{\Omega}\frac{\partial A}{\partial t}d\Omega+\frac{\sigma}{l}u=0 \tag{7}$$

$$\frac{l}{SM}\sum_{m=1}^{M}\iint_{\Omega^{(m)}}\frac{\partial A^{(m)}}{\partial t}d\Omega+\frac{l}{\sigma S}i+u=0 \tag{8}$$

where σ is the conductivity of the material; S is the cross-sectional area of the rotor bars; l is the axial length of the bar; u is the potential differences between the two ends of the rotor bars and i is the rotor bar current. The electrical circuit equations of the rotor end rings should be coupled into the FEM model and hence u can be eliminated first [6].

Because the iron cores are laminated, the eddy currents in the iron cores are neglected in the mathematical model. Therefore the field equation in the iron domains and in the air-gap is:

$$\nabla \times (\nu \nabla \times A) = 0 \tag{9}$$

By using FEM formulation, one obtains the large non-linear global system of equations as follows [5]:

$$[C][A \quad i]^T + [D]\left[\frac{\partial A}{\partial t} \quad \frac{\partial i}{\partial t}\right]^T = [P] \tag{10}$$

where the unknowns $[A]$ and $[i]$ are, respectively, the magnetic vector potentials and currents; $[C]$, $[D]$ are the coefficient matrices and $[P]$ is the vector associated with the input a.c. stator phase voltages and the d.c. stator currents. The Backward Euler's method is used to discretize the time variables. The rotor FEM mesh is moved in accordance with the rotation of the rotor.

IV. Computation of Losses

After the waveforms of currents are computed, the copper loss in the stator windings can be directly obtained from:

$$P_{Cu1} = \frac{1}{N_{step}}\sum_{k=1}^{N_{step}}\left(i_A^2 + i_B^2 + i_C^2\right)R_1 \tag{11}$$

where i_A, i_B and i_C are stator phase currents in the three phases. The copper loss in the rotor bars is:

$$P_{bar} = \frac{1}{N_{step}}\sum_{k=1}^{N_{step}}\sum_{i=1}^{N_{element}}\frac{j^2}{\sigma}S_i l \tag{12}$$

where $N_{element}$ is the number of elements in the rotor bars; j is current density in rotor bars and S_i is the area of element i. The copper loss in the rotor end ring is:

$$P_{ring} = \frac{1}{N_{step}}\sum_{k=1}^{N_{step}}\sum_{i=1}^{N_{bar}} i_i^2 R_{ring} \tag{13}$$

where N_{bar} is the number of rotor bars; i_i is the end-ring current of the i^{th} bar and R_{ring} is the resistance of the rotor ring.

The average value of the eddy-current loss in W/m^3 in one cycle is [7]:

$$p_{eav} = \frac{1}{T}\int_0^T \sigma_c\left(\frac{1}{\sqrt{2}\pi}\frac{\mathrm{d}B}{\mathrm{d}t}\right)^2 \mathrm{d}t \tag{14}$$

where T is the period of the fundamental waveform and the coefficient σ_c is obtained from the characteristics of material. In the time stepping FEM $\mathrm{d}B/\mathrm{d}t$ can be replaced by $(B^k - B^{k-1})/\Delta t$ and the flux density B at each element can be obtained. Thus the total eddy-current loss of the motor is:

$$P_{eav} = \frac{1}{N_{step}}\sum_{k=1}^{N_{step}}\sum_{i=1}^{N_{element}}\sigma_c\left(\frac{1}{\sqrt{2}\pi}\frac{B_i^k - B_i^{k-1}}{\Delta t}\right)^2 S_i l \tag{15}$$

where N_{step} is the number of time steps in one period T; $N_{element}$ is the number of elements in the iron cores; B_i^k and B_i^{k-1} are the magnetic flux densities of element i at the k^{th} and k-1$^{\text{th}}$ step, respectively; l is the length of the iron core and Δt is the time step size. Fourier analysis is not necessary in each step.

Because the waveforms of the magnetic flux density in each element are known, the hysteresis loss in W/m^3 can be found directly from:

$$p_{hav} = (1/T)\oint H\mathrm{d}B = (\text{area of hysteresis loop } B)/T \tag{16}$$

V. Results

The afore-mentioned FEM modeling has been used to simulate the phantom loading and the normal loading operation of a skewed rotor induction motor (11 kW / 380 V, 50 Hz, 4 poles, 48 stator slots, 44 rotor slots, Δ connection). The time step size is 0.038 ms. The rotor is divided into 4 slices. The number of total unknowns of the FEM equations is 5394 and the average solution time of each time stepping needs 15 s on a Pentium II / 300 MHz. A typical computed stator current waveform and the corresponding measured one are shown in Fig. 5 and Fig. 6, respectively.

It was found by the computation and experiments that the closest simulation of the actual operating condition occurs when the phantom current is in the ratio of 1:1:1 at which the phantom current I_{dc} flowing in the phases is:

$$\sqrt{I_{dc}^2 + I_{ac}^2} = I_N \tag{17}$$

where I_{dc} is the d.c. current injected into the motor windings; I_{ac} is the a.c. no-load r.m.s. current flowing in the motor windings and I_N is the rated r.m.s. current of the motor. This means that the effective current on phantom loading is the same as the rated r.m.s. current of the machine. For the phantom loading test with the d.c. current flowing in the three phases in the ratio of 1:1:0, the phantom current I_{dc} should be:

$$\sqrt{(2/3)I_{dc}^2 + I_{ac}^2} = I_N \tag{18}$$

A comparison of computed losses between phantom loading and full-load operation is as shown in Table I. The results of the computation confirm that only very small differences appear in the loss distribution between phantom loading and normal loading. Because the main component of the fields is excited by the a.c. voltage with the suggested phantom loading schemes (refer to Fig. 7), the iron losses will be close to that at full-load. However, the injected d.c. currents will not just produce copper loss in the stator windings, it also induces a.c. currents in the rotor cage (refer to Fig. 8). Because these currents tends to cancel each other, and the relative speed between the rotor cage and the d.c. field is nearly synchronous, the currents in the rotor cage will be very close to their rated values. A comparison of temperature-rise tests between phantom loading and direct operation is shown in Table II. The experimental work shows that the results of the proposed temperature-rise method are surprisingly close to that of the normal direct loading method.

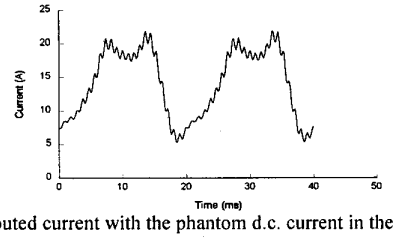

Fig. 5 Computed current with the phantom d.c. current in the ratio of 1:1:0

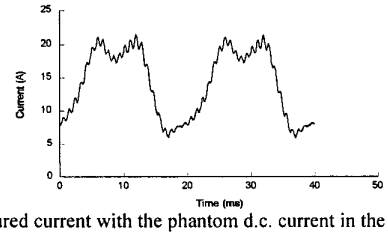

Fig. 6 Measured current with the phantom d.c. current in the ratio of 1:1:0

VI. Conclusion

Phantom loading provides a convenient way to assess the temperature-rise of induction motors. The proposed multi-slice 2-D time stepping FEM is an effective means to understand the physics and the order of magnitude of the various losses under phantom loading. The results also give a good indication as which connection should be used in order to produce an accurate simulation of the real full-load condition. The findings reported in this paper therefore provide a solid basis for those intending to use phantom loading to assess the thermal properties of their induction motors.

TABLE I
Comparison of Computed Losses Between Phantom Loading Operations and Full-Load Operations (W)

	Phantom 1:1:1	Phantom 1:1:0	Full-load
Stator Copper Loss	586.0	586.5	584.4
Rotor Copper Loss	241.6	257.7	263.2
Stator Eddy-current Loss	84.1	84.4	80.1
Stator Hysteresis Loss	86.6	86.9	83.7
Rotor Eddy-current Loss	93.5	92.5	80.3
Rotor Hysteresis Loss	45.1	46.3	5.4
Total	1136.9	1154.3	1097.1

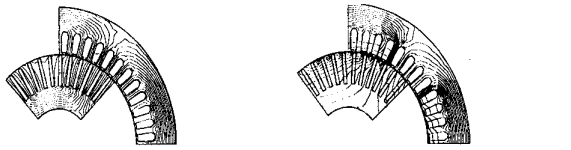

(a) With both a.c. and d.c. exciting
Difference between lines: 2.21×10^{-3} Wb/M

(b) With only d.c. exciting
Difference between lines: 0.22×10^{-3} Wb/M

Fig. 7 Flux distribution for phantom loading with the d.c. current in the ratio of 1:1:0

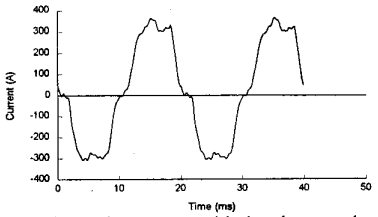

Fig. 8 Computed rotor bar current with the phantom d.c. current in the ratio of 1:1:0

TABLE II
Comparison of Temperature-Rise Measurements Between Phantom Loading and Full-Load Direct-Loading (K)

Method	Temperature-rise
Phantom 1:1:1 loading	61.7
Phantom 1:1:0 loading	61.9
Standard full-load	62.8

References

[1] W. Fong, "New Temperature Test for Polyphase Induction Motors by Phantom Loading," *Proc. IEE*, vol. 119, No.7, 1972, pp.883-888.

[2] S. L. Ho, "Further Development of Phantom Loading in Induction Motors," *International Conference on Electrical Machines*, IEE, U.K., 15-17 Sept., 1992, pp.298-302.

[3] S. L. Ho, "Study of Stray Losses under Phantom Loading Conditions in Induction Motors," *International Conference on Electrical Machines*, Paris, France, 5-8 Sept., 1994, pp.548-553.

[4] S. L. Ho and W. N. Fu, "Review and Further Application of Finite Element Methods in Induction Motors," *Electric Machines and Power Systems*, Taylor & Francis, Vol.26, No.2, 1998, pp.111-125.

[5] S. L. Ho and W. N. Fu, "A Comprehensive Approach to the Solution of Direct-Coupled Multislice Model of Skewed Rotor Induction Motors Using Time-stepping Eddy-Current Finite Element Method," *IEEE Transactions on Magnetics*, vol. 33, No.3, May, 1997, pp.2265-2273.

[6] A. Arkkio, "Analysis of induction motors based on the numerical solution of the magnetic field and circuit equations," *Helsinki, Acta Poly. Scandinavica, Elect. Engineering Series*, no. 59, 1987, pp.1-63

[7] S. L. Ho, W. N. Fu and H. C. Wong, "Estimation of Stray Losses of Skewed Induction Motors Using Coupled 2-D and 3-D Time Stepping Finite Element Methods," *IEEE Trans. Magn.*, Vol.34, No.5, September, 1998, pp. 3102-3105.